

The Causal Structure of Dynamical Charged Black Holes

Sungwook E. Hong,^{*} Dong-il Hwang,[†] Ewan D. Stewart, and Dong-han Yeom[‡]

Department of Physics, KAIST, Daejeon, 305-701, South Korea

(Dated: May 29, 2019)

We study the causal structure of dynamical charged black holes by numerical simulations. Without Hawking radiation, there exists inner horizon which is the same with null Cauchy horizon with mass inflation singularity. However, when we include the Hawking radiation, the inner horizon bends in space-like direction, and the Cauchy horizon will be separated from the inner horizon. As time goes on, because of the pair-creation, the black hole loses its charge, and finally transits to a neutral black hole; we also have demonstrated the charged-neutral transition of a charged black hole. Around the inner horizon, the mass function is finite, and so regular and penetrable; but, since the curvature functions become trans-Planckian, we cannot say more about the region beyond the inner horizon, and it is natural to say that there is a “physical” space-like singularity even if we consider the Hawking radiation. However, as long as we assume a large number of scalar fields, we can say that our results are trustworthy even beyond the inner horizon; in this case, the cosmic censorship and the black hole complementarity can be violated.

PACS numbers: 04.70.Dy, 04.20.Dw, 04.25.dc, 04.40.Nr, 04.62.+v

I. INTRODUCTION

A charged black hole is a quite well-known solution, since the black hole physics began [1]. However, although its geometrical structure of static solution was well understood [2], there still remained some interesting questions.

For example, a charged black hole has the time-like singularity, and it may imply that there exist causally undetermined regions. The boundary between the determined and undetermined regions is called the Cauchy horizon [3]. If there exists a Cauchy horizon, it may imply that there exist some regions which cannot be determined from the past. However, some authors argued that there are somehow local effects along the Cauchy horizon like the infinite blue shift [4]. Then, any observer will hardly penetrate the Cauchy horizon, and it seemed to rescue a philosophical idea known as *the strong cosmic censorship* [3].

At first, some authors had already observed that the Hawking radiation makes the inner horizon unstable in semi-classical analysis [5]. Moreover, after a pioneering work of Poisson and Israel [6], now we understand that the inner horizon must be interpreted as a kind of curvature singularity: if there exists an energy flow along the inner horizon, and if an observer crosses it, he will feel infinite energy. This effect is known as *the mass inflation*; it makes a curvature singularity along the inner horizon, and makes it unstable.

However, there still remain some questions: *whichever it is stable or unstable, anyway, in what sense?* Some authors argued that, the inner horizon is unstable, and it may collapse to the singularity at the center [7]. Oth-

ers said that since the inner horizon is problematic, there should be no inner horizon in real situations by some effects [8] (also, see [9]). Others argued, although the inner horizon has some problems like a curvature singularity, it is still stable, and the inside structure seems to be safe: in the sense that, the metric perturbation is finite and the tidal deformation is small enough [10][11]. In some contexts, some authors argued that, there are two kinds of singularities, strong and weak singularity [12], and the inner horizon becomes a weak and null singularity [13]: that is, one observer possibly hits the inner horizon first, and then, collapses to the strong singularity deep inside of the black hole [14]. However, all of these results are based on a charged black hole without Hawking radiation.

To figure out which opinion is correct and which is not, we need to understand the causal structure of charged black holes for not only static cases, but also *dynamical cases*. Of course, there are some previous researches which tried to consider the Hawking radiation, but those calculations could not include the mass inflation effect until 1998 [19] — until then, they tried to calculate near extreme limit (the motivation came from the information loss problem) with some approximations [15], or used the Vaidya metric which may too simple [16][17]. Reproducing the whole dynamical evolution from flat space-time to curved space-time became possible only after computing power was sufficiently increased. Pioneering simulations were done by previous researchers [18][19][20][21][22](see also [8]), whose methods we tried to follow.

We assume the spherical symmetry, and set up proper equations for Maxwell and scalar fields with Hawking radiation. For more realistic situations, we should have included the pair-creation effect [8][20] (and analytically, [23][24]), but for our purposes, it is enough to exclude the pair-creation effect for some reasons explained below. After reproducing the same results of previous authors,

^{*}Electronic address: eastm@muon.kaist.ac.kr

[†]Electronic address: eastone83@gmail.com

[‡]Electronic address: innocent@muon.kaist.ac.kr

we could do our own experiments about charged black holes with Hawking radiation.

From these simulations, we will answer following questions:

- What is the proper Penrose diagram for dynamical charged black holes with Hawking radiation?
- Is the inner horizon stable or unstable? Is the inner horizon penetrable or not? Can we extend the classical general relativity beyond the inner horizon?
- Are there any problems with the cosmic censorship and the black hold complementarity?

In Section II, we describe our numerical and experimental setup. In Section III, we report the results of our simulation. And, in Section IV, the implications and the comparison to other opinions are discussed. Remark that we will use conventions of [2] since it is convenient to describe the simulation scheme.

II. NUMERICAL SETUP

A. Basic Schemes

We describe the gauge-invariant Lagrangian with a complex massless scalar field ϕ and an electromagnetic gauge field A_μ [2]:

$$\mathcal{L} = -(\phi_{;a} + ieA_a\phi)g^{ab}(\bar{\phi}_{;b} - ieA_b\bar{\phi}) - \frac{1}{8\pi}F_{ab}F^{ab}, \quad (1)$$

where $F_{ab} = A_{b;a} - A_{a;b}$, and e is the unit charge. From this Lagrangian we can derive the equations of motion for the scalar field and the electromagnetic field:

$$\phi_{;ab}g^{ab} + ieA^a(2\phi_{;a} + ieA_a\phi) + ieA_{a;b}g^{ab}\phi = 0,$$

$$\frac{1}{2\pi}F_a{}^b{}_{;b} - ie\phi(\bar{\phi}_{;a} - ieA_a\bar{\phi}) + ie\bar{\phi}(\phi_{;a} + ieA_a\phi) = 0. \quad (2)$$

Also, the energy-momentum tensor becomes

$$\begin{aligned} T_{ab} = & \frac{1}{2}(\phi_{;a}\bar{\phi}_{;b} + \bar{\phi}_{;a}\phi_{;b}) + \frac{1}{2}(-\phi_{;a}ieA_b\bar{\phi} \\ & + \bar{\phi}_{;b}ieA_a\phi + \bar{\phi}_{;a}ieA_b\phi - \phi_{;b}ieA_a\bar{\phi}) \\ & + \frac{1}{4\pi}F_{ac}F_b{}^c + e^2A_aA_b\phi\bar{\phi} + \frac{1}{2}\mathcal{L}g_{ab}. \end{aligned} \quad (3)$$

Now, we will describe our numerical set up. We followed schemes of some previous works (especially, we followed [25]). We start from the double-null coordinate (our convention is $[u, v, \theta, \phi]$),

$$ds^2 = -\alpha^2(u, v)dudv + r^2(u, v)d\Omega^2, \quad (4)$$

assuming the spherical symmetry. From this coordinate, we can write the Einstein equation with scalar field and Maxwell field, as well as one-loop order semiclassical effect.

Because of the gauge symmetry, we can choose the gauge field as $A_\mu = (a, 0, 0, 0)$ with a single function a [21]. We define main functions as follows (conventions came from [19][20][21]): the metric function α , the radial function r , the Maxwell field a , and the complex massless scalar field $s \equiv \sqrt{4\pi}\phi$. And, we use some conventions: $d \equiv \alpha_v/\alpha$, $h \equiv \alpha_u/\alpha$, $f \equiv r_u$, $g \equiv r_v$, $w \equiv s_u$, $z \equiv s_v$, where B_u means the partial derivatives of B with respect to u . From these setup, following components can be calculated:

$$G_{uu} = -\frac{2}{r}(f_u - 2fh),$$

$$G_{uv} = \frac{1}{2r^2}(4rf_v + \alpha^2 + 4fg),$$

$$G_{vv} = -\frac{2}{r}(g_v - 2gd),$$

$$G_{\theta\theta} = -4\frac{r^2}{\alpha^2}\left(d_u + \frac{f_v}{r}\right),$$

$$T_{uu} = \frac{1}{4\pi}(w\bar{w} + iea(\bar{w}s - w\bar{s}) + e^2a^2s\bar{s}),$$

$$T_{uv} = \frac{a_v^2}{4\pi\alpha^2},$$

$$T_{vv} = \frac{1}{4\pi}z\bar{z},$$

$$T_{\theta\theta} = \frac{r^2}{4\pi\alpha^2}\left((w\bar{z} + z\bar{w}) + iea(\bar{z}s - z\bar{s}) + \frac{2a_v^2}{\alpha^2}\right). \quad (5)$$

From the equations of the scalar field and the Maxwell field, we get following equations:

$$\begin{aligned} rz_u + fz + gw + iearz + ieags + ies\frac{\alpha^2q}{4r} = 0, \\ \left(\frac{r^2a_v}{\alpha^2}\right)_v + \frac{ier^2}{4}(z\bar{s} - s\bar{z}) = 0. \end{aligned} \quad (6)$$

In the second equation, it is convenient to define $q \equiv 2r^2a_v/\alpha^2$; it is easy to verify that q can be interpreted as the electric charge in our scheme. Then, all a_v s in previous equations can be expressed as a function of r, α , and q .

We also consider one-loop order semiclassical effect. Because of the spherical symmetry, it is reasonable to use the 2-dimensional results (which should be divided

by $4\pi r^2$.) [26]:

$$\begin{aligned}\langle T_{uu} \rangle &= \frac{P}{4\pi r^2} (h_u - h^2), \\ \langle T_{uv} \rangle &= \langle T_{vu} \rangle = -\frac{P}{4\pi r^2} d_u, \\ \langle T_{vv} \rangle &= \frac{P}{4\pi r^2} (d_v - d^2),\end{aligned}\quad (7)$$

with $P \equiv N l_{pl}^2$, where N is the number of massless scalar fields generating the Hawking radiation and l_{pl} is the Planck length. By changing P , we can tune the strength of quantum effect. Also, P determines the relation between the number of massless scalar fields and the typical length scale of our simulation.

Finally, we use the semiclassical Einstein equation,

$$G_{\mu\nu} = 8\pi(T_{\mu\nu} + \langle T_{\mu\nu} \rangle). \quad (8)$$

Including this, we can list enough equations for the simulation.

A. *Einstein equations:*

$$\begin{aligned}d_u &= \frac{1}{(1 - P/r^2)} \left(\frac{fg}{r^2} + \frac{\alpha^2}{4r^2} - \frac{\alpha^2 q^2}{2r^4} \right. \\ &\quad \left. - \frac{1}{2}(w\bar{z} + \bar{w}z) - \frac{iea}{2}(s\bar{z} - \bar{s}z) \right),\end{aligned}\quad (9)$$

$$g_v = 2dg - rz\bar{z} - \frac{P}{r}(d_v - d^2), \quad (10)$$

$$f_v = -\frac{fg}{r} - \frac{\alpha^2}{4r} + \frac{\alpha^2 q^2}{4r^3} - \frac{P}{r} d_u. \quad (11)$$

B. *Maxwell equations:*

$$a_v = \frac{\alpha^2 q}{2r^2}, \quad (12)$$

$$q_v = -\frac{ier^2}{2}(\bar{s}z - s\bar{z}). \quad (13)$$

C. *Scalar field equations:*

$$z_u = -\frac{fz}{r} - \frac{gw}{r} - \frac{iearz}{r} - \frac{ieags}{r} - \frac{ie}{4r^2}\alpha^2 qs, \quad (14)$$

$$w_v = z_u. \quad (15)$$

D. *Definitions:*

$$\alpha_v = \alpha d, \quad (16)$$

$$r_v = g, \quad (17)$$

$$s_v = z. \quad (18)$$

We can substitute Equation (9) to Equation (11). Also, we can substitute Equation (14) to Equation (15). Then all equations contain only one derivative, except Equation (10). We can integrate r from these equations by two independent ways: one can get g from Equation (10) to get r ; one can get g from Equation (11) (since $f_v = g_u$) to get r . Analytically these methods are equivalent; thus, we used these independent ways to check the consistency of our calculation. Since (10) contains two different derivatives and one of them should be calculated by approximation, we usually used (11) to calculate g . We solved these equations successively with the 4th order Runge–Kutta method [27]. Remark that, there is a singularity around $r = \sqrt{P}$ in Equation (9); since it depends on the one-loop order approximation scheme, we may regard it as the central singularity; notice that \sqrt{P} is fixed and very small compared to the typical length scale of our simulation.

B. Initial Conditions

We need initial conditions for ten functions on $u = \text{const} = u_i = 0$ and $v = \text{const} = v_i = 0$ surfaces. There are two kinds of information: geometry(α, r, g, d, f) and matter(s, w, z, a, q).

On the geometry side, we have gauge freedom to choose initial r function; although all constant u and v lines are null, there remains freedom to choose the distances between these null lines. We choose $r(u, v_i) = ur_{u0} + r_0$ and $r(u_i, v) = vr_{v0} + r_0$. Then, $g(u_i, v) = r_{v0}$ and $f(u, v_i) = r_{u0}$ are naturally obtained.

Because of the spherical symmetry, we use a shell-shaped scalar field and its inside does not affected by this shell. Thus, we can simply choose $q(u, v_i) = 0$, $a(u, v_i) = 0$ and $\alpha(u, v_i) = 1$. Moreover, since the mass function($M(u, v) = (r/2)(1 + q^2/r^2 + 4r_u r_v/\alpha^2)$) [28] should vanish at this initial surface, we can choose $r_{u0} = -1/2$, $r_{v0} = 1/2$. According to Equation (13), if we represent the scalar field as $s = |s| \exp(i\theta)$, $q_v = er^2 |s|^2 \theta_v$ holds. Therefore, it is quite natural to define the initial pulse of scalar field as:

$$s(u_i, v) = A \sin^2 \left(\pi \frac{v - v_i}{v_f - v_i} \right) \exp \left(\pm 2\pi i \frac{v - v_i}{v_f - v_i} \right),$$

where v_f defines the width of the pulse, A is a free parameter to determine the amplitude, and the sign of the exponent determines the sign of charge. Then, we naturally get $z(u_i, v)$ from its definition. We may assume that there is no field amplitude for initial v_i surface, from which we get $w(u, v_i) = 0$. Also from Equation (10), we can regard $d = rz\bar{z}/2g$ for u_i surface, since we can assume that there is no Hawking effect on the initial surface.

If one wants to add another pulse, one can extend these initial schemes to the additional pulse with s_1, z_1 , and w_1 . Since the equations for s ((14) and (15)) are linear on s and its derivatives, one can solve the scalar field

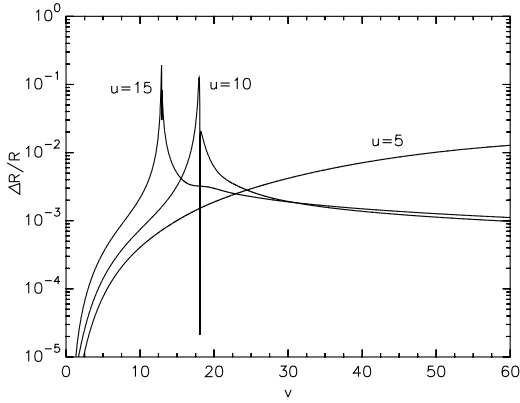


FIG. 1: Difference between two integration schemes for r function along a few constant u lines.

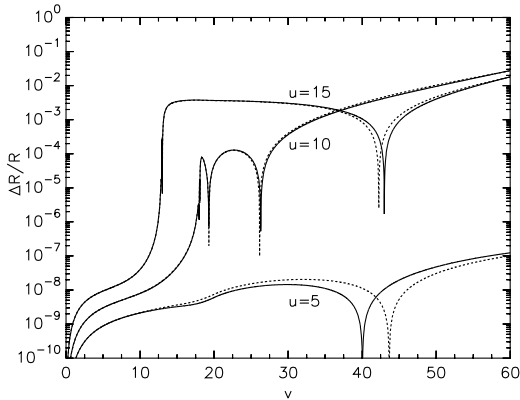


FIG. 2: Plot of $|1 \text{ times } - 2 \text{ times}|$ (normal lines); and $|2 \text{ times } - 4 \text{ times}| \times 4$ (dotted lines) for a few constant u lines of r function. Our simulation converges to second order.

equations independently for the first pulse and the second pulse; in this way, one can observe the dynamics of each pulse independently. Of course, the scalar fields in other equations should be regarded as the whole field amplitude like $s = s_0 + s_1$.

By integrating some equations, we can get enough information for initial surfaces. Then, it is possible to integrate all domains. Remark that, we choose $r_0 = 10$ and $v_f = 20$. Therefore, if we fix 3 parameters (e, P, A) , we can specify one simulation.

C. Consistency and Convergence Check; Adaptive Grid Refinement Method

To check the consistency, we used two independent ways to integrate r function, using (10) or (11) as mentioned above. For a standard simulation, we used $(e, P, A) = (0.1, 0.1, 0.25)$. Figure 1 shows that the dif-

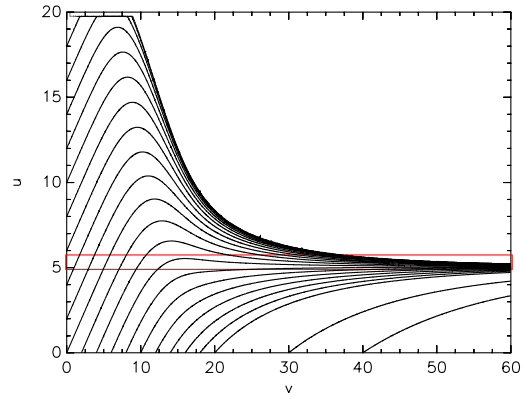


FIG. 3: Contour diagram of r function for a Schwarzschild black hole; $(0, 0.1, 0.25)$. One can observe space-like singularity structure.

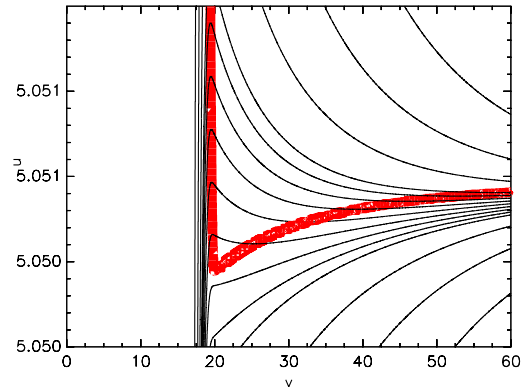


FIG. 4: Detailed plot of the box in Figure 3. One can see that the outer horizon ($r_v = 0$, thick line) bends in time-like direction as the matter supply ends.

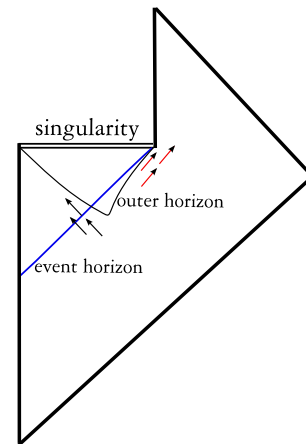


FIG. 5: Theoretically predicted causal structure [29]. Previous results confirm this diagram. A thin curved line is the apparent horizon, and a thin straight line is the event horizon.

ference between two schemes is less than $\sim 1\%$ (except near the horizons and the singularity; these regions are handled by an additional method discussed below). This consistency is quite meaningful; we observed that a single change of any equations can easily break this consistency.

To check the convergence, we compared the calculated results using different step sizes; 1 times, 2 times, and 4 times for each axis. The difference between 1 times and 2 times should be proportional to the difference between 2 times and 4 times. We observed that this difference increases about 4 times as the step size becomes twice (Figure 2; thus, our simulation seems to converge to second order [21]). Similar to the consistency case, this difference increases rapidly around the horizons.

One may guess that the error of $\sim 1\%$ is not satisfiable. If we are not interested in the structures around the horizons and the singularity, we do not have to worry about this error scale; however, we need more precise calculations since we want to check more details around these regions. This error comes from bad choices of functions in some sense; for example, the radial function r folds badly around the outer horizon, and the metric function α decays exponentially beyond the inner horizon. Thus, if one wants to calculate more precisely and efficiently, the adaptive grid refinement method (AGM) [21] is an attractive solution. We choose the step size Δu adaptively so that the ratio of change of r and r itself ($r_u \Delta u / r$) to be constant, as well as $\alpha_u \Delta u / \alpha$. Moreover, since the equations (9) and (11) become singular around $r = \sqrt{P}$, we need to arrange $r_{uv} \Delta u \Delta v / r$ and $\alpha_{uv} \Delta u \Delta v / \alpha$ to be constant. This resolves the problem of convergence by a significant order.

Finally, we checked whether this simulation gives a physically true picture for a Schwarzschild black hole case [20]. Then, we need to choose $e = 0$; $(e, P, A) = (0, 0.1, 0.25)$. Figure 3 and 4 are contour diagrams for r , and show the dynamics of outer horizon $r_v = 0$. As the matter collapses, the outer horizon bends in space-like direction; after the matter collapsing ends, because of the Hawking radiation, the outer horizon bends in time-like direction. These phenomena are consistent with known facts about local horizons [29][30]. Moreover, one can see a space-like central singularity (where $r = \sqrt{P}$ and some functions diverge) structure. This confirms that our simulation gives a quite physical result for, at least, a Schwarzschild case (Figure 5).

III. RESULTS

A. Without Hawking Radiation; Previous Results

For a static case, the charged black hole solution is quite well-known. The following is the classical vacuum

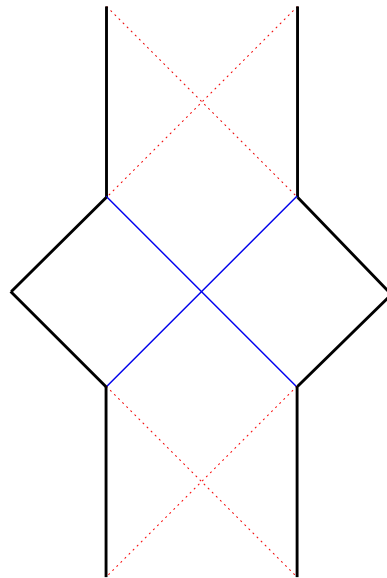


FIG. 6: The Penrose diagram of static charged black holes for $m > q$. Thick diagonal lines are future and past infinities. Thick vertical lines are central singularities. Dotted lines are the inner horizon (and, also the Cauchy horizon). And, the normal lines are the outer horizon (and, also the event horizon).

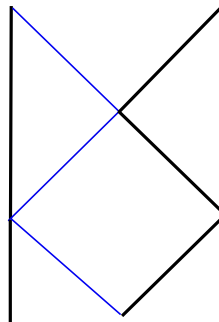


FIG. 7: The Penrose diagram of static charged black holes for $m = q$. In this case, the outer horizon is the same with the inner horizon.

solution:

$$ds^2 = - \left(1 - \frac{2m}{r} + \frac{q^2}{r^2} \right) dt^2 + \left(1 - \frac{2m}{r} + \frac{q^2}{r^2} \right)^{-1} dr^2 + r^2 d\Omega^2, \quad (19)$$

where m is the mass, and q is the electric charge. From this metric, we can draw a maximally extended causal structure, and get the Penrose diagram for this static charged black hole solution [2] (Figure 6 and Figure 7). However, these diagrams themselves are not true for dynamical situations. Firstly, similar to the Schwarzschild case, real situations do not have time symmetrical metric structures. The initial state is generally flat, and the

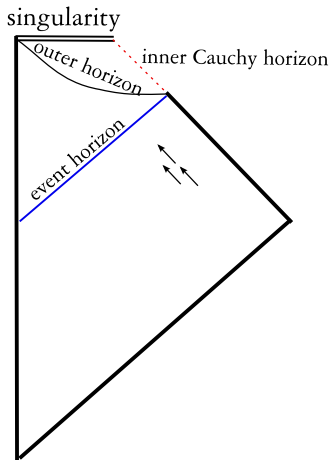


FIG. 8: Charged black holes with mass inflation. The collapsing matter generates the mass inflation and the space-like singularity. A normal diagonal straight line is the event horizon, and a diagonal dotted straight line is the inner Cauchy horizon. A thin curved line is the outer horizon.

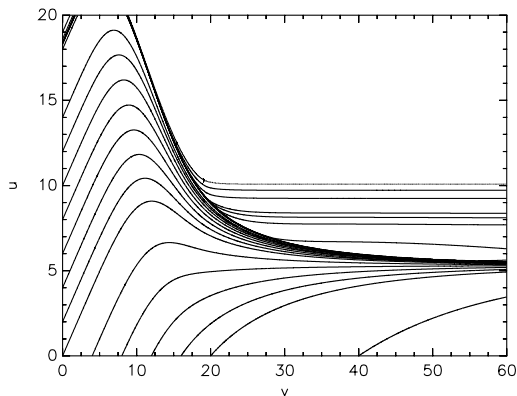


FIG. 9: Contour diagram of r function for $(0.1, 0, 0.25)$. This diagram confirms Figure 8. The outer horizon ($r_v = 0$) grows in space-like direction, and the inner horizon (also, $r_v = 0$) would be located at $v \rightarrow \infty$ limit.

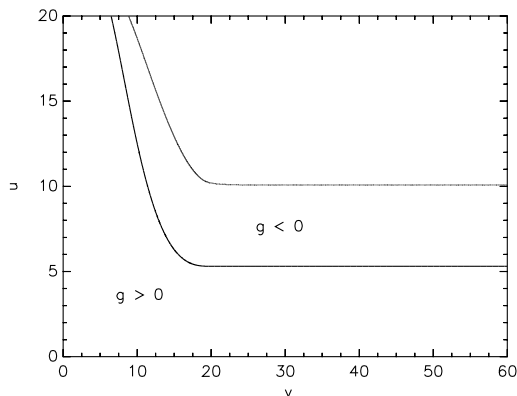


FIG. 10: The outer horizon ($g = r_v = 0$) for $(0.1, 0, 0.25)$.

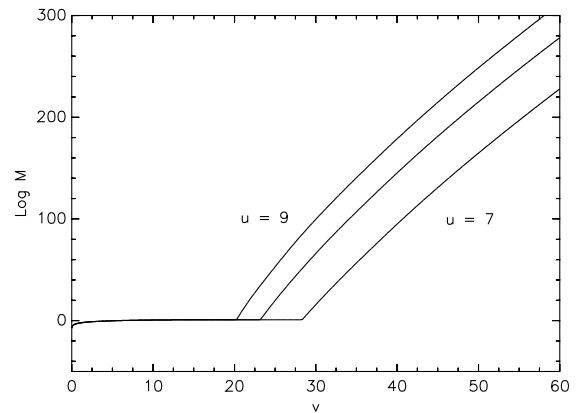


FIG. 11: Log plot of mass function along a few constant lines ($u = 7, 8, 9$). Obviously, it blows up exponentially; clear signature of the mass inflation.

final state will be flat again in many cases.

Then, one may ask a question: what will happen if we push some charged matter to flat space-time? One simple guess is the growth of outer and inner horizons, and the evolution of time-like singularity [16]. However, because of the mass inflation [6][19], this will not happen. The inner horizon must have grown from zero radius, but, because of the mass inflation, it cannot grow, and it becomes the central singularity. This singularity will be space-like, not time-like, since the inner horizon seems to be collapsed in some sense. Thus, we may guess the Penrose diagram in Figure 8, and it had confirmed by some numerical simulations [20] [21], and we reproduced it (9 and 10, where we used $(e, P, A) = (0.1, 0, 0.25)$).

To check whether the inner horizon becomes singular or not, we need to check the behavior of the mass function. The mass function of our scheme is $M(u, v) = (r/2)(1 + q^2/r^2 + 4r_u r_v/\alpha^2)$ [28]. Figure 11 shows the behavior of the mass function; it blows up exponentially as $v \rightarrow \infty$. This is a typical signature of the mass inflation; $M \sim \exp(\kappa_i v)$, where κ_i is the surface gravity of the inner horizon [6]. Then, some scalar quantities like the Ricci scalar and the Kretschmann scalar ($K \equiv R_{\alpha\beta\gamma\delta}R^{\alpha\beta\gamma\delta} \sim M^2$) become infinity as $v \rightarrow \infty$ [10]. Remark that, since we did not consider the quantum effect, the Planckian cutoff of scalar curvatures can be regarded as ∞ . Thus, the curvature singularity occurs at the $v \rightarrow \infty$ limit. We may need further check that, whether the inner horizon becomes a kind of strong singularity or weak singularity [10]; but, as we include the Hawking radiation, this problem becomes trivial in some sense (discussed in subsection III F).

B. With Hawking Radiation;

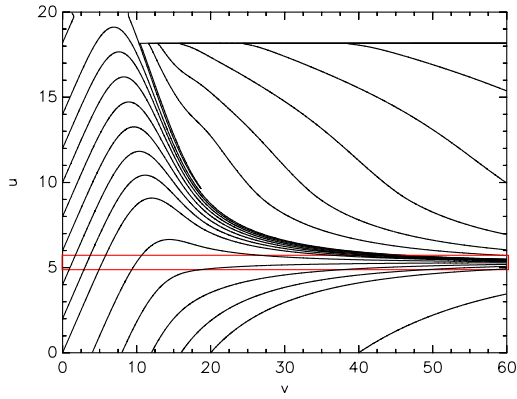


FIG. 12: Contour diagram of r function for $(0.1, 0.1, 0.25)$. Note that r function starts to increase from the inner horizon.

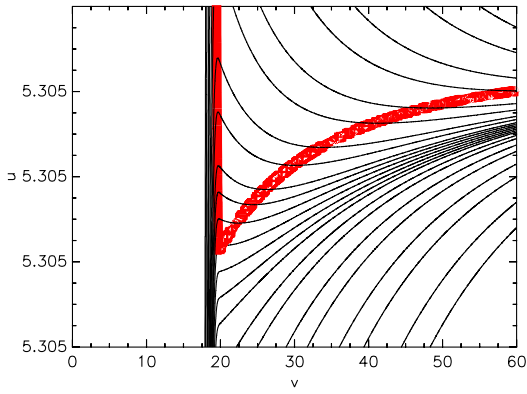


FIG. 13: Detailed plot of the box in Figure 12.

Space-like Bending of Inner Horizon and appearance of Cauchy horizon

Now we consider the Hawking radiation; $(e, P, A) = (0.1, 0.1, 0.25)$. Figure 12, 13, 14 and 15 show the contour diagrams of r , r_v and r_u . One can interpret that the inner horizon ($r_v = 0$) bends in space-like direction, and $r_u = 0$ contour is almost the same with the inner horizon. The inner horizon is space-like, and not null: this result is the same with [20], but is different from some traditional interpretations about the inner horizon, e.g., [10][14][19]. The radial function r behaves consistently with f and g ; r slightly increases for any observers who fall beyond the inner horizon.

One interesting feature is a null cutoff line at the top of these diagrams. We observed r function along this cutoff line, shown in Figure 16. This figure shows a sharp point around $r = 0.3 \approx \sqrt{P}$; the central singularity. Moreover, the cutoff line has regular r value, in contrast to Figure 9 where the cutoff line is the central singularity. Thus, although this cutoff line itself is regular, the region beyond cannot be calculated because of the singularity in Figure 16, whose values are needed to calculate this region; *this null section grows from singularity*. Therefore, we can

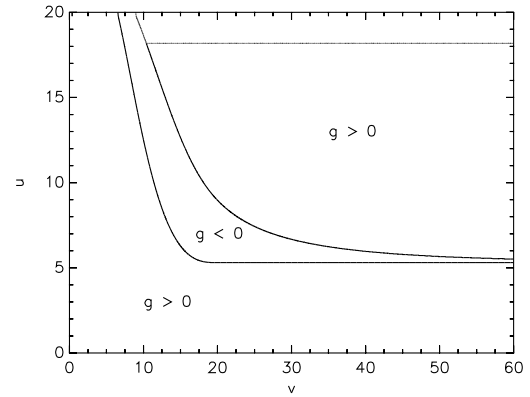


FIG. 14: The outer and inner horizons ($g = r_v = 0$) for $(0.1, 0.1, 0.25)$.

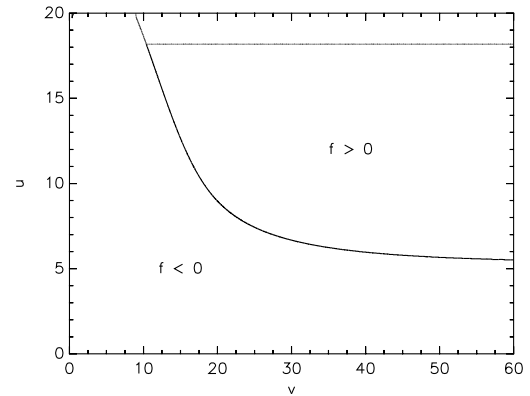


FIG. 15: $f = r_u = 0$ contour for $(0.1, 0.1, 0.25)$.

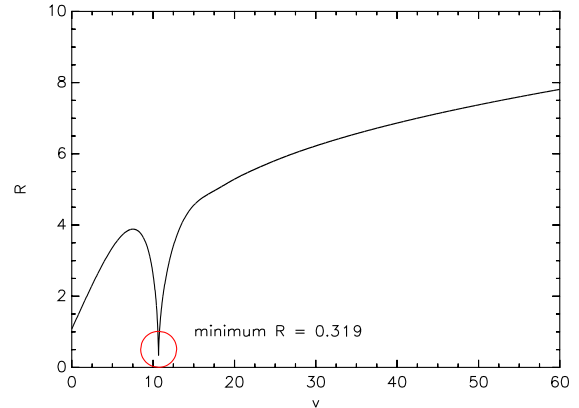


FIG. 16: A section of r function around the null cutoff line ($u \approx 17.5$). The sharp point has $r \approx 0.319$, which is near the central singularity. It confirms that this cutoff line is the Cauchy horizon.

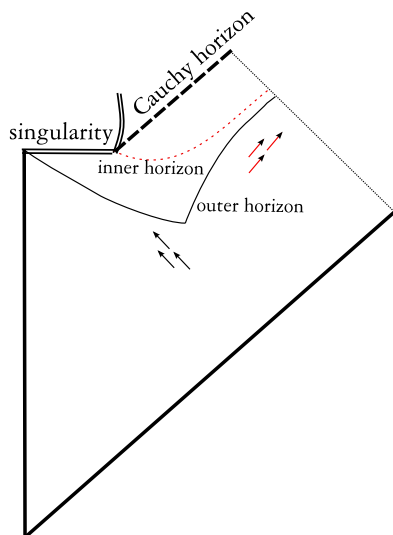


FIG. 17: The Penrose diagram for Figure 12. A normal curved line is the outer horizon, and a dotted curved line is the inner horizon.

interpret this null cutoff line as *the Cauchy horizon* by definition. Now, the inner horizon is separated from the Cauchy horizon; this is a very new feature confirmed by our simulation.

In fact, these features (space-like bending of the inner horizon, and appearance of the Cauchy horizon) can be predicted in this sense; to connect the non-extreme Penrose diagram (Figure 6) to the extreme one (Figure 7), the only possible way is the time-like bending of the outer horizon, and the space-like bending of the inner horizon [15]. This expectation is the same with some known facts about local horizons (e.g., [30]). However, our results are better in this point: some of previous authors tried to paste the near extreme limit (Figure 6) to the extreme one (Figure 7) [15]; but, *we tried to paste the mass inflation scenario to the extreme one*, or Figure 8 to Figure 7. Then, the only possible way is the space-like bending of the inner horizon; and the time-like singularity (of static limit) will make the Cauchy horizon. Then, the Cauchy horizon will be separated from the inner horizon, and returns to our result.

Finally, we can draw a schematic diagram in Figure 17. We will discuss the mass function and the properties of inner horizon in the following subsections.

C. Dependence on Initial Conditions

Figure 12 shows general features of charged black holes, but some details can be affected by initial conditions. We can choose the initial conditions for the mass-charge ratio, as well as the length and time scale of evolution. These factors can be tuned by three parameters e , P , and A . From throughout research, we could figure out the general behavior of contour diagrams. Initial conditions

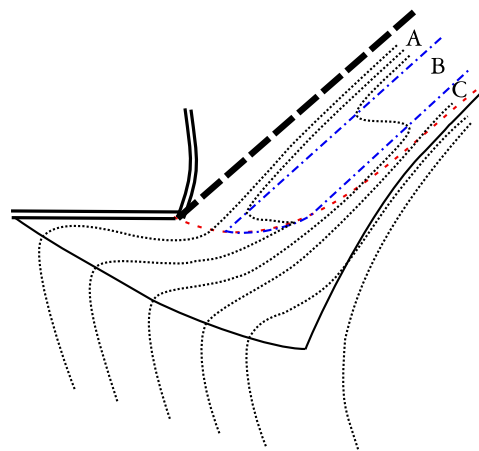


FIG. 18: A characteristic plot of r -contour lines. A normal thin curve line and a thin dashed curved line are $g = 0$ contour, i.e., outer and inner horizons; a dash-dot curved line is $f = 0$ contour. Dotted lines are contour lines of r function; they increase from left to right. Region A and C are for $(f < 0, g > 0)$, and region B is for $(f, g > 0)$.

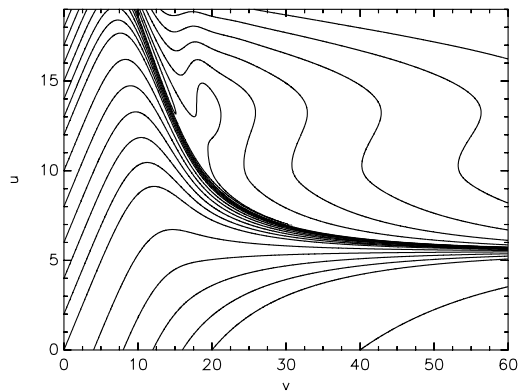


FIG. 19: Contour diagram of r function for $(e, P, A) = (0.13, 0.1, 0.25)$. One can see regions like B, C, and B again in Figure 18.

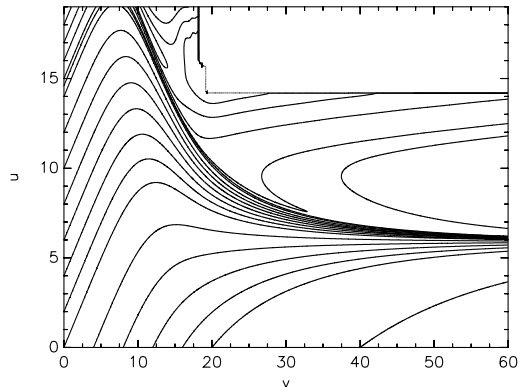


FIG. 20: Contour diagram of r function for $(e, P, A) = (0.17, 0.1, 0.25)$. One can see regions like A and B.

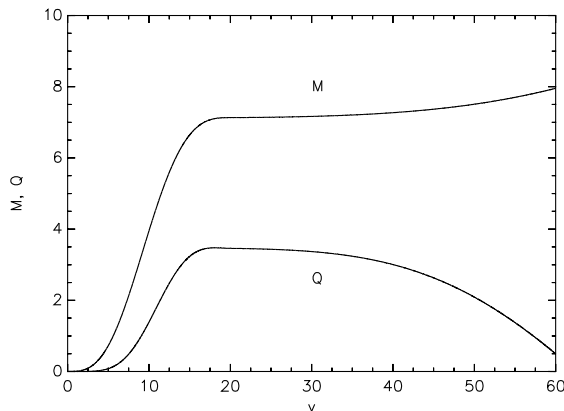


FIG. 21: Asymptotically calculated charge and mass change during the neutralization. Because of the oppositely charged matter, the charge decreases to almost 0, whereas the mass increases slightly; we may assume that the increase of mass would not affect the qualitative behaviors of causal structure.

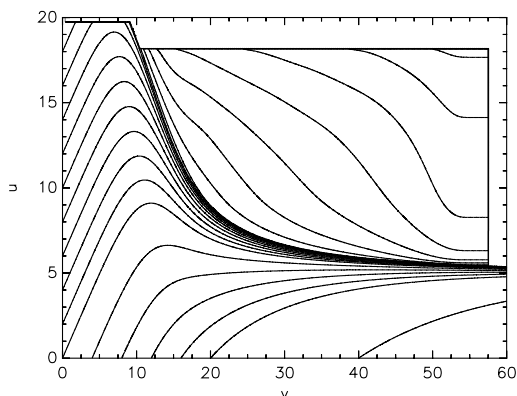


FIG. 22: Contour diagram of r function for a possible charged–neutral transition. Note that there is another cut-off line along u direction.

do not change the qualitative behaviors of g contour, or the horizon structure; but it does change f contour.

Figure 18 shows the characteristic behaviors of r contours, which is consistent with [20]. Choosing initial conditions determines our scope of view, which is restricted by the location of Cauchy horizon and the time scale of evolution; if the Cauchy horizon is too close to the inner horizon, one cannot see the region A, and if the time evolution is too slow, one cannot see the region C; Figure 12 shows this case. Since the detailed structure does not affect the qualitative behaviors of the horizon structure, we chose the simplest one. The other examples are Figure 19 and 20.

D. Charged–Neutral Transition

Now we observe the aspects of transition from a charged black hole to a neutral black hole. In fact, we

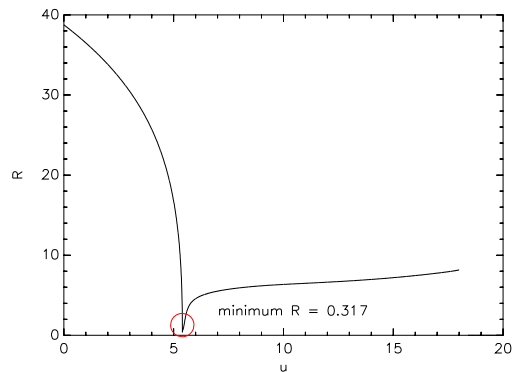


FIG. 23: A section of r function around the null cutoff line ($v \approx 57$) near the transition point. It confirms that this cutoff line also is the Cauchy horizon.

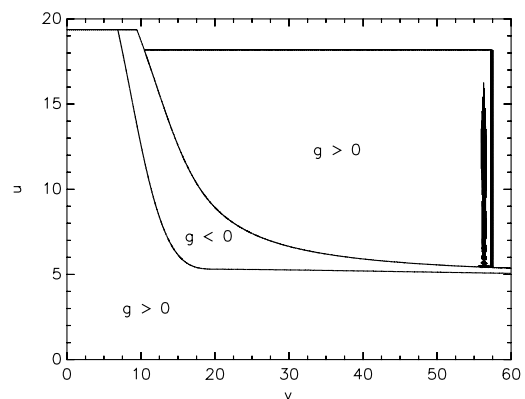


FIG. 24: The outer and inner horizons ($g = r_v = 0$) for the charged–neutral transition. Inside of the inner horizon, since r function converges to some fixed values along v direction, there is some fuzzy regions. Also, there arises the central singularity at the end of the inner horizon.

should have included discharging effect at the very first; however, it can be ignored for some reasons. Firstly, there are some results that if we push charged matter quickly, discharging effect during the collapse is not significant [20]. On the other hand, if the discharging effect is stronger than the other effects during the collapse, the black hole becomes a neutral one; then, its causal structure is trivial in some sense, and not our interests. Secondly, after the black hole is formed, if the pair creation ratio is in the strongly suppressed regime [31], the Hawking radiation will induce the black hole to the extreme state; this case is consistent with our previous results. If it is not suppressed, the charged black hole will transit to a neutral one; the results in this subsection qualitatively deal with this case.

If the charge itself is large enough, the pair creation ratio is suppressed, and the black hole stably approaches to an extreme one. However, an extreme black hole cannot be regarded as an eternal remnant. In general, a charged black hole will approach to an extreme limit; and, dis-

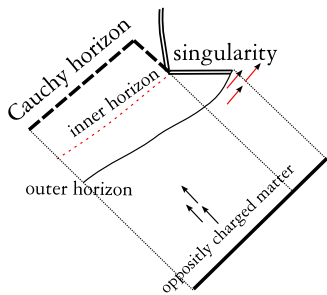


FIG. 25: The Penrose diagram for charged–neutral transition. A normal curved line is the outer horizon, and a dotted curved line is the inner horizon.

charging and Hawking effect will make its charge and mass smaller and smaller. One possibility is that it approaches to a stable one; the other possibility is that the pair–creation neutralizes the black hole, which is possible since the charge–mass ratio of some elementary particles are quite large. Then, since a neutral black hole has a finite lifetime, it will be totally evaporated. Moreover, if we push some oppositely charged matter into the black hole, we can make it neutral artificially. Therefore, in any possible scenarios, we need to check the causal structure of charged–neutral transition to see the final stage of a charged black hole.

The charged–neutral transition can be simulated by supplying oppositely charged matter to a charged black hole. After the black hole is formed, we supplied an additional field with almost the same amount of opposite charge and relatively small mass; in considering another field, we used the technique mentioned in subsection II B, so that we can analyze the behavior of secondary field independently in subsection III F. As we push this matter slowly, the total charge decreases significantly (it need not be 0; there is some smooth transition region of charge, between the space–like singularity and the time–like singularity [32].), and the mass increases slightly (Figure 21). We may regard this experiment as a good approximation of general charged–neutral transition; firstly, this process itself is realizable in principle, and secondly, since the mass change is not significant, we may assume that it is qualitatively the same with the pair–creation effect.

In Figure 22, as the charge of the black hole decreases, there arises another cutoff line along u direction. From the similar argument to the previous one (Figure 23, compared to Figure 16), one can convince that this cutoff line also is the Cauchy horizon by definition. As one can see in Figure 24, the singularity in Figure 23 arises at the end of the inner horizon; it is quite natural since the inner horizon is the extremum of r function along v direction. When the charged–neutral transition happens, the result for a charged black hole (Figure 12) should be changed to that for a neutral one (Figure 3) in some way. Then, the region beyond the inner horizon in Figure 12 should be disappeared, and the singularity in Figure 3

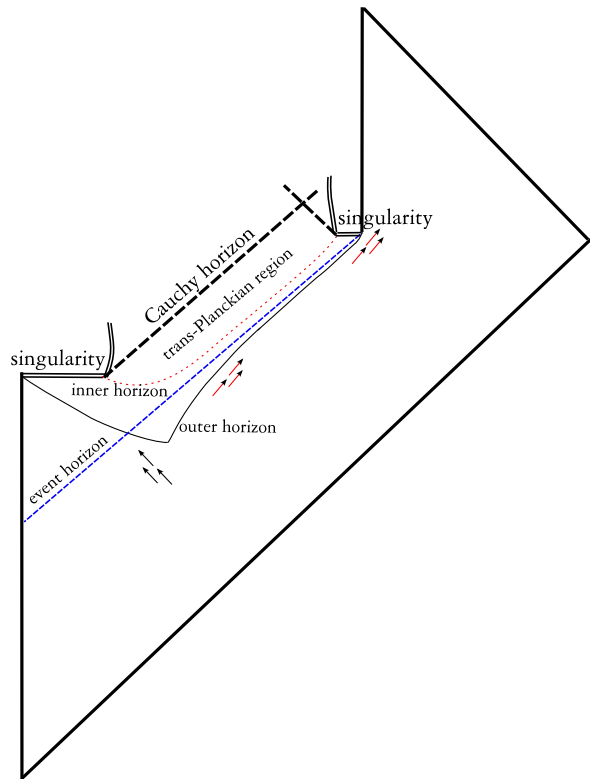


FIG. 26: The causal structure of dynamical charged black holes.

should be constructed; in our result, the inner horizon changed to this singularity, and the Cauchy horizon from this singularity cuts out the region beyond the inner horizon, and accomplishes the transition process. Finally, we can draw the causal diagram for this process, Figure 25. There were some pioneer studies to describe the charged–neutral transition with Vaidya metric [17]; their results seem to be consistent with ours.

E. The Causal Structure of Dynamical Charged Black Holes

Now we can draw the causal structure of dynamical charged black holes. Figure 26 is the integrated result of Figure 17 and Figure 25. One can see the outer horizon and the inner horizon structures, as well as the Cauchy horizon.

We found that, there arises a trans–Planckian region around the inner horizon where the curvature functions blow up beyond the Planckian cutoff; this problem will be discussed in subsection III G. However, the inner horizon is not singular but regular in *general relativistic sense*; as discussed in following subsections, it is geodesically complete and penetrable. Thus, if one is allowed to extend the general relativity beyond the inner horizon, our results contain more implications; this induces some in-

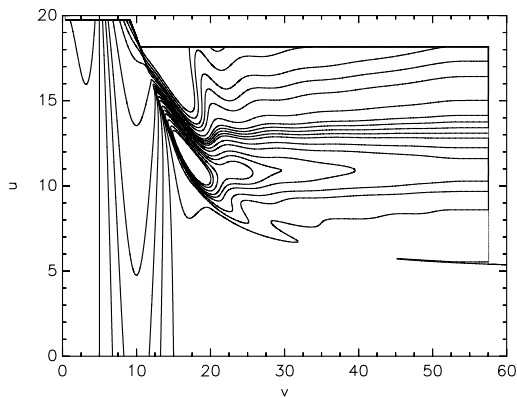


FIG. 27: Contour diagram of $\text{Re } s_0$ which is used to form the black hole in Figure 22. It flows to form a black hole, and bends along the inner horizon.

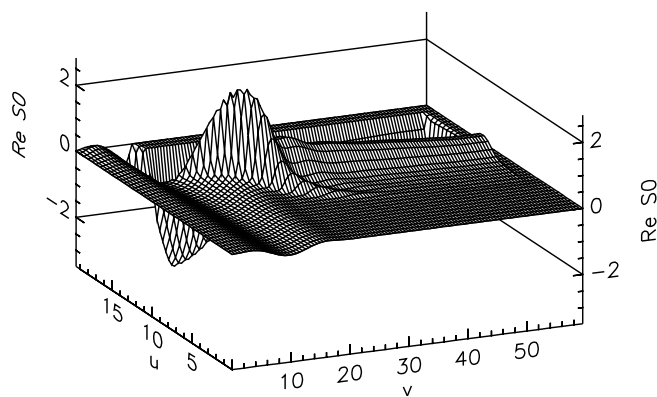


FIG. 28: 3D diagram of $\text{Re } s_0$.

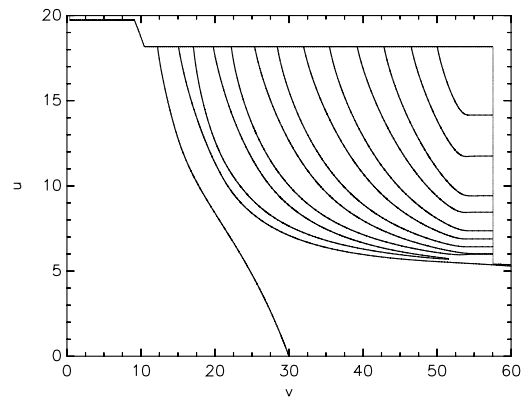


FIG. 29: Contour diagram of $\text{Re } s_1$ which is used to neutralize the black hole. It is affected by the inner horizon, but obviously penetrates the inner horizon.

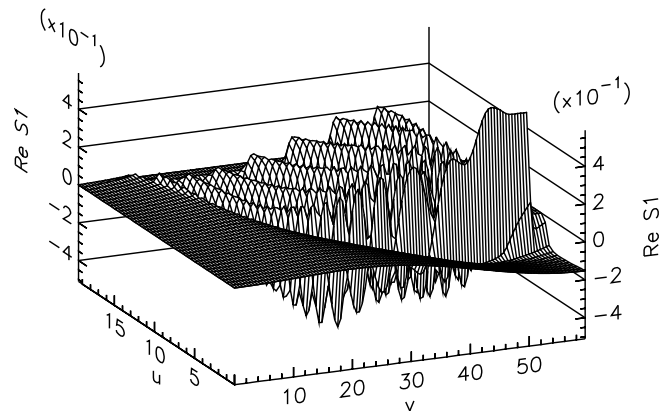


FIG. 30: 3D diagram of $\text{Re } s_1$.

teresting ideas.

F. Penetrability of Inner Horizon

At first, we check the penetrability of inner horizon. We can use the simulated results for the charged–neutral transition, since we supplied additional pulse to the black hole there. The first pulse makes the black hole, and the second one gradually neutralizes it; since we can calculate their dynamics independently, we observed whether the second pulse can penetrate the inner horizon or not.

Figure 27 and 28, as well as 29 and 30, show the behaviors of each pulse. In these diagrams, one can see that the inner horizon actually has some barrier property; field configurations change drastically near the inner horizon. But still, the inner horizon is penetrable; fields penetrate the inner horizon, and flow beyond it. Remark that the field amplitude increases beyond the inner horizon; the radial function near the inner horizon becomes quite small and it seems to affect the field amplitude. We discussed that the detailed structure near the inner horizon depends on initial conditions (Figure

18). For strong perturbations, the sensitivity of the inner horizon is different among these regions; region B is quite stable, while A and C are more unstable [34]. But this does not affect the qualitative nature of regularity and penetrability of the inner horizon.

Moreover, as discussed in the next subsection, although the mass function starts to increase near the inner horizon, it is still finite for all domains. Thus, the inner horizon itself and the region beyond the inner horizon are regular and penetrable in general relativistic sense; *this simply reflects the weak nature of the inner Cauchy horizon singularity when there is no Hawking radiation* [10].

G. Analysis of Mass Function; Mass Inflation and Trans-Planckian Problem

Now we observe the mass function. Figure 31 and 32 show the behavior of mass function along a few constant u and v lines. Around the inner horizon, the mass function starts to blow up exponentially, which is a typical signature of the mass inflation [19][21]. Although the

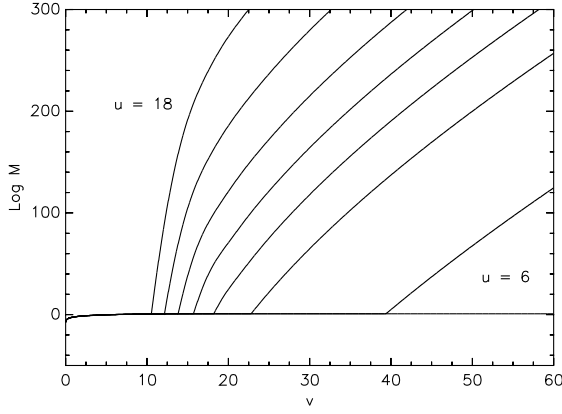


FIG. 31: Log plot of mass function along a few constant u lines ($u = 6, 8, 10, 12, 14, 16, 18$) for Figure 12. It blows up exponentially; clear signature of the mass inflation.

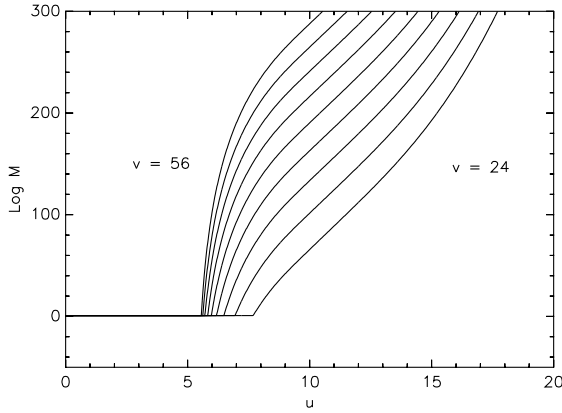


FIG. 32: Log plot of mass function along a few constant v lines ($v = 24, 28, 32, 36, 40, 44, 48, 52, 56$). Mass inflation is observed in both null directions.

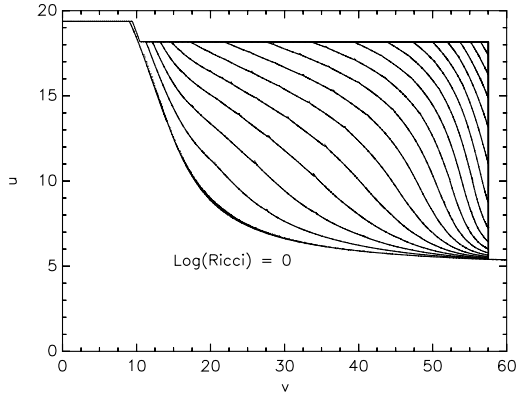


FIG. 33: Contour diagram of Log Ricci scalar for the charged–neutral transition. It starts to blow up exponentially near the inner horizon.

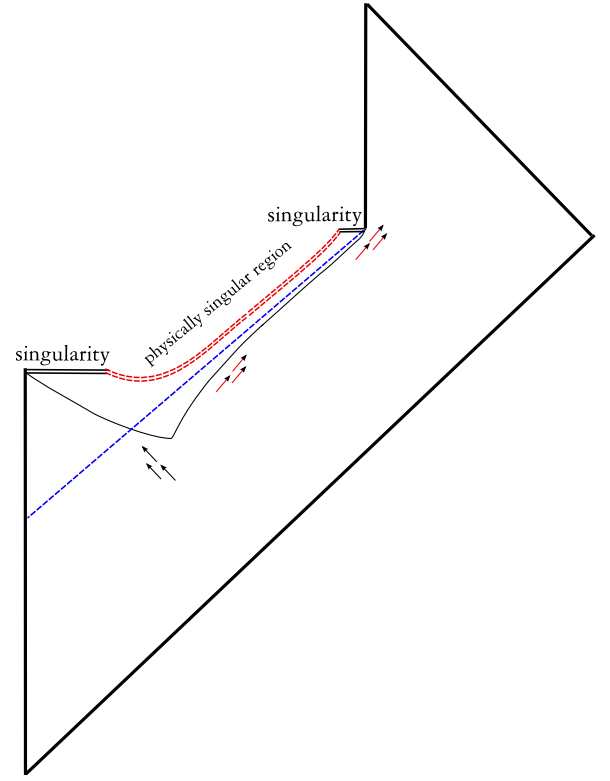


FIG. 34: The causal structure of dynamical charged black holes for a suitable number of massless scalar fields. It is natural to interpret that there is a kind of physically singular region around the inner horizon; however, it is regular in general relativistic sense, and inherits the nature of weak singularity.

mass function blows up, there is no signature of infinite divergence except the central singularity, $r = \sqrt{P}$; it is still finite even near the Cauchy horizon. Thus, as long as we rely on the general relativity, the strong cosmic censorship can be violated.

However, since we have considered quantum effect, we should also consider the Planck scale. And it turns out that, along with the mass function, some curvature functions also blow up exponentially (Figure 33): as the metric function α decays exponentially beyond the inner horizon, the mass function ($\sim 1/\alpha^2$), the Ricci scalar ($\sim 1/\alpha^2$), and the Kretschmann scalar ($\sim 1/\alpha^4$) blow up exponentially together. If they increase beyond the Planckian cutoff, it will be problematic. As discussed in subsection II A, parameter $P \equiv Nl_{pl}^2$ determines the relation between the number of massless scalar fields N and the Planck length scale l_{pl} of our simulation. Thus, although we have fixed P , the Planckian cutoff of scalar curvature $\sim 1/l_{pl}^2$ can be chosen arbitrarily, as long as we choose large N .

However, if N is physically bounded, we cannot avoid the trans-Planckian curvature problem. In this case, if we should regard this trans-Planckian inner horizon as a kind of singularity, its causal structure becomes Figure

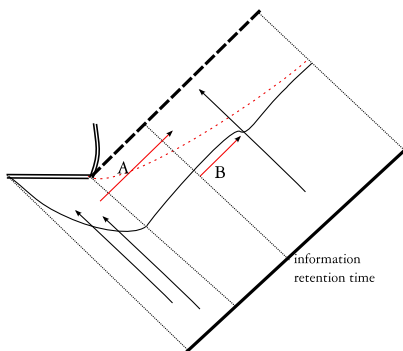


FIG. 35: A schematic diagram for the duplication experiment. An in-falling observer sends his information to the out-going direction (A); his information is also contained in the Hawking radiation (B). If the region beyond the inner horizon is regular, a second observer can see both information and violate the no cloning theorem.

34. It is quite similar to some dilatonic black hole models [33]; the inner horizon is the same with the physical singularity which has non-zero radius, and it approaches to a stable extreme black hole. Note that there are some differences: as discussed above, the inner horizon in our model is regular in general relativistic sense, so that it is geodesically complete and penetrable. In natural situations with suitable N , Figure 34 will be a reliable causal structure of charged black holes.

On the other hand, if one assume large N , the whole region in Figure 26 becomes reliable except the central singularity. One may think that this assumption is not natural in real situations; however, it is still unclear whether it is impossible or not. At the bottom, the causal structure depends on N because the strength of the Hawking radiation can be changed by an adjustable value N ; without changing any fundamental properties like the Planck constant, we can consider a charged black hole with intensive Hawking radiation without any trans-Planckian regions. Thus, if there is no fundamental reason to exclude the large number of field, we should check some ideas which would not depend on some phenomenological opinions like N . The authors think that some important examples can be the cosmic censorship and the black hole complementarity.

H. Cosmic Censorship and Black Hole Complementarity

Some authors guessed that the weak cosmic censorship can be violated in charged black holes [16]. However, those authors used the Vaidya metric which may be too simple. The simulation scheme we have used considers full evolution of charged black holes, and shows that the weak cosmic censorship simply holds. However, the strong cosmic censorship seems not in general. When there is no Hawking radiation, the mass function

diverges at the inner Cauchy horizon; this resolves the problem. But if we consider the Hawking radiation, since the mass function is finite at the Cauchy horizon, we may regard that the strong cosmic censorship is violated. However, we also observed that the trans-Planckian curvature arises around the inner horizon in real situations. Then, one may guess that we cannot extend our physics beyond the inner horizon; there would be essentially no problem with the strong cosmic censorship, except large N limit.

We think that this conclusion is not bad to the cosmic censorship; although it can be violated in some limit, since that limit is not realistic, it is enough to believe that philosophical idea. For example, in the weak cosmic censorship case, if we push some electrons to an extreme charged black hole, we may see the naked singularity which violates the weak cosmic censorship; however, this experiment is not natural for some reasons [35], and thus, we regard that it is very difficult to see a naked singularity in our universe and the weak cosmic censorship holds. Our results show that the strong cosmic censorship will hold in this sense.

Finally, we will check an idea related to the information loss problem; the black hole complementarity [31][36]. According to the black hole complementarity, after the information retention time (when the initial area of the black hole decreases to its half value), an observer outside of the black hole can see the information of the in-falling matter from the Hawking radiation. However, since the free-falling information does not affected by the Hawking radiation, two copies of information may exist; it seems to violate the no cloning theorem of quantum mechanics. The black hole complementarity argues that it is not a problem since these two copies cannot be observed by a single observer.

To check whether one observer can see both information or not, one may think a gedanken-experiment. One observer A free-falls into the black hole and sends his information to the out-going direction right after he crosses the event horizon. After the information retention time, the other observer B sees the information of A from the Hawking radiation, and go into the black hole to get the information which A sent to him; thus, B seems to observe both of the information. However, in the neutral black hole case, to deliver information to B before it collapses to the singularity, A should send a signal with energy $\sim \exp M^2$ which is greater than the black hole mass itself; thus, this process is impossible. This argument also holds for charged black holes with causal structure Figure 34; A should send a signal with large energy to deliver his information to B before it collapses to the physically singular inner horizon.

However, in our model, the duplication experiment is possible in large N limit (Figure 35). Since A can send signal beyond the inner horizon, he has enough time so that the signal does not need large energy (as discussed in subsection III F, penetration of a pulse across the inner horizon is possible.). Thus, B can get the informa-

tion from A at the region beyond the inner horizon; B 's world line and the signal's world line definitely meet each other. The black hole complementarity can be violated in this case; however, the authors think that there are some ideas to rescue the complementarity [37].

Although we need large N limit, if the complementarity is a fundamentally true idea, it seems to be independent of the choice of N , unless this limit is fundamentally forbidden. If the large N is improbable in real situations, this experiment may be impossible in practice; but, there still remains a question since the complementarity depends on some phenomenological properties, which seem to be independent of the idea itself. We may need to check whether this large N limit is impossible even in the string theory.

IV. DISCUSSION

We made a proper model of charged black holes with complex scalar field and gauge field by assuming the spherical symmetry. We included $1 + 1$ dimensional approximation of a renormalized energy momentum tensor to consider the quantum effect. From numerical simulations we could find a proper Penrose diagram for dynamical charged black holes (Figure 26). There may exist some dependence on initial conditions, but still we found some definite features: space-like bending of the inner horizon, as well as the separation between the Cauchy horizon and the inner horizon. Also we have demonstrated a proper process of the charged-neutral transition: generation of the Cauchy horizon and the singularity.

There were some traditions to regard the inner Cauchy horizon as a null curvature singularity. However, we demonstrated that the inner horizon is not the same with the Cauchy horizon in general, and it is not a curvature singularity in general relativistic point of view; it is stable against small perturbations, as well as regular and penetrable. One potential problem is the curvature beyond the inner horizon which blows up beyond the Planckian

cutoff. Thus, in general, we cannot extend physics beyond the inner horizon even though it is regular in general relativistic sense; this reflects the mass inflation and the weak nature of the curvature singularity when there was no Hawking radiation. Now it is fair to say that, *in natural situations, a charged black hole has "physical" space-like singularity even in dynamical cases* (Figure 34). In this case, although the Cauchy horizon is regular in general relativistic sense, the region beyond the inner horizon, including the Cauchy horizon, is beyond our knowledge; the strong cosmic censorship can be satisfied.

However, if we can assume a large number of scalar fields, we may trust our results beyond the inner horizon. Although this assumption is not realistic, it can be applied to some fundamental ideas which would not depend on this phenomenological choice. We found that the strong cosmic censorship and the black hole complementarity can be violated in this limit.

Some interesting features of charged black holes (like a worm hole or a generation of a bubble universe) should be checked in our model, as well as more detailed analysis for the dependence on initial conditions [34]. Moreover, we may extend the analysis to some other string inspired models like dilatonic black holes. We may include the cosmological constant in our model; this may be helpful for the trans-Planckian problem [38], but it must be tested carefully.

Acknowledgments

The authors would like to thank Evgeny Sorkin, Changsub Shin, Heeseung Zoe, and Yuree S. Lim for discussions and encouragements. This work was supported by BK21 and the Korea Research Foundation Grant funded by the Korean government. And also, the authors thank to the Korea Science and Engineering Foundation(KOSEF) grant funded by the Korea government.

-
- [1] H. Reissner, Ann. Physik., **50**, 106 (1916); G. Nordstrom, Proc. Kon. Ned. Akad. Wet., **20**, 1238 (1918).
 - [2] S. W. Hawking and G. F. R. Ellis, "*The large scale structure of space-time*," Cambridge, Cambridge University Press (1973).
 - [3] R. M. Wald, "*General relativity*," Chicago, Univ. Pr. (1984).
 - [4] M. Simpson and R. Penrose, Int. J. Theor. Phys. **7**, 183 (1973); S. Chandrasekhar and J. B. Hartle, Proc. R. Soc. Lond. A **384**, 301 (1982).
 - [5] W. A. Hiscock, Phys. Rev. D **15**, 3054 (1977); N. D. Birrell and P. C. W. Davies, Nature **272**, 35 (1978); Y. Gursel, V. D. Sandberg, I. D. Novikov and A. A. Starobinsky, Phys. Rev. D **19**, 413 (1979).
 - [6] E. Poisson and W. Israel, Phys. Rev. D **41**, 1796 (1990).
 - [7] M. L. Gnedin and N. Y. Gnedin, Class. Quantum Grav. **10**, 1083 (1993).
 - [8] A. V. Frolov, K. R. Kristjansson and L. Thorlacius, Phys. Rev. D **72**, 021501(R) (2005) [arXiv:hep-th/0504073]; A. V. Frolov, K. R. Kristjansson and L. Thorlacius, Phys. Rev. D **73**, 124036 (2006) [arXiv:hep-th/0604041]; L. Thorlacius, J. Korean Phys. Soc. **50**, S1 (2007) [arXiv:hep-th/0607048].
 - [9] A. Ori, arXiv:gr-qc/0609092.
 - [10] A. Ori, Phys. Rev. Lett. **67**, 789 (1991); A. Ori, Phys. Rev. Lett. **68**, 2117 (1992).
 - [11] L. M. Burko, Phys. Rev. D **66**, 024046 (2002) [arXiv:gr-qc/0206012].

- [12] F. J. Tipler, Phys. Lett. **64A**, 8 (1977).
- [13] L. M. Burko, Phys. Rev. Lett. **79**, 4958 (1997) [arXiv:gr-qc/9710112]; L. M. Burko and A. Ori, Phys. Rev. D **57**, R7084 (1998) [arXiv:gr-qc/9711032]; L. M. Burko, Phys. Rev. D **59**, 024011 (1998) [arXiv:gr-qc/9809073].
- [14] A. Bonanno, S. Droz, W. Israel and S. M. Morsink, Phys. Rev. D **50**, 7372 (1994) [arXiv:gr-qc/9403019].
- [15] S. P. Trivedi, Phys. Rev. D **47**, 4233 (1993) [arXiv:hep-th/9211011]; A. Strominger and S. P. Trivedi, Phys. Rev. D **48**, 5778 (1993) [arXiv:hep-th/9302080]; D. A. Lowe and M. O’Loughlin, Phys. Rev. D **48**, 3735 (1993) [arXiv:hep-th/9305125]; T. Jacobson, Phys. Rev. D **57**, 4890 (1998) [arXiv:hep-th/9705017]; K. Diba and D. A. Lowe, Phys. Rev. D **65**, 024018 (2001) [arXiv:hep-th/0107137]; K. Diba and D. A. Lowe, Phys. Rev. D **66**, 024039 (2002) [arXiv:hep-th/0202005].
- [16] Y. Kaminaga, Class. Quant. Grav. **7**, 1135 (1990); M. K. Parikh and F. Wilczek, Phys. Lett. B **449**, 24 (1999) [arXiv:gr-qc/9807031].
- [17] O. Levin and A. Ori, Phys. Rev. D **54**, 2746 (1996).
- [18] T. Piran and A. Strominger, Phys. Rev. D **48**, 4729 (1993) [arXiv:hep-th/9304148]; R. Parentani and T. Piran, Phys. Rev. Lett. **73**, 2805 (1994) [arXiv:hep-th/9405007]; S. Ayal and T. Piran, Phys. Rev. D **56**, 4768 (1997) [arXiv:gr-qc/9704027].
- [19] S. Hod and T. Piran, Phys. Rev. Lett. **81**, 1554 (1998) [arXiv:gr-qc/9803004]; S. Hod and T. Piran, Gen. Rel. Grav. **30**, 1555 (1998) [arXiv:gr-qc/9902008].
- [20] E. Sorkin and T. Piran, Phys. Rev. D **63**, 084006 (2001) [arXiv:gr-qc/0009095]; E. Sorkin and T. Piran, Phys. Rev. D **63**, 124024 (2001) [arXiv:gr-qc/0103090].
- [21] Y. Oren and T. Piran, Phys. Rev. D **68**, 044013 (2003) [arXiv:gr-qc/0306078].
- [22] J. Hansen, A. Khokhlov and I. Novikov, Phys. Rev. D **71**, 064013 (2005) [arXiv:gr-qc/0501015].
- [23] A. Ori, Phys. Rev. D **63**, 104016 (2001) [arXiv:gr-qc/0102067].
- [24] V. P. Frolov, W. Israel and S. N. Solodukhin, Phys. Rev. D **54**, 2732 (1996) [arXiv:hep-th/9602105].
- [25] R. S. Hamade and J. M. Stewart, Class. Quant. Grav. **13**, 497 (1996) [arXiv:gr-qc/9506044].
- [26] P. C. W. Davies, S. A. Fulling and W. G. Unruh, Phys. Rev. D **13**, 2720 (1976).
- [27] W. H. Press, S. A. Teukolsky, W. T. Vetterling and B. P. Flannery, “*Numerical Recipes: The Art of Scientific Computing*,” 3rd ed. Cambridge, Cambridge University Press (2007).
- [28] B. Waugh and K. Lake, Phys. Rev. D **34** 2978 (1986).
- [29] S. W. Hawking, Commun. Math. Phys. **43**, 199 (1975) [Erratum-ibid. **46**, 206 (1976)].
- [30] A. Ashtekar and B. Krishnan, Living Rev. Rel. **7**, 10 (2004) [arXiv:gr-qc/0407042]; S. A. Hayward, arXiv:gr-qc/9303006; S. A. Hayward, Phys. Rev. D **70**, 104027 (2004) [arXiv:gr-qc/0408008].
- [31] L. Susskind and J. Lindesay, “*An introduction to black holes, information and the string theory revolution: The holographic universe*,” Hackensack, World Scientific (2005).
- [32] L. M. Burko, Phys. Rev. Lett. **90**, 121101 (2003) [Erratum-ibid. **90**, 249902 (2003)] [arXiv:gr-qc/0209084].
- [33] D. Garfinkle, G. T. Horowitz and A. Strominger, Phys. Rev. D **43**, 3140 (1991) [Erratum-ibid. D **45**, 3888 (1992)].
- [34] S. E. Hong, D. Hwang and D. Yeom, in preparation.
- [35] N. D. Birrell and P. C. W. Davies, “*Quantum fields in curved space*,” Cambridge, Cambridge University Press (1982).
- [36] L. Susskind, L. Thorlacius and J. Uglum, Phys. Rev. D **48**, 3743 (1993) [arXiv:hep-th/9306069]; L. Susskind and L. Thorlacius, Phys. Rev. D **49**, 966 (1994) [arXiv:hep-th/9308100];
- [37] D. Hwang, D. Yeom and H. Zoe, in preparation.
- [38] E. Poisson, [arXiv:gr-qc/9709022].